

BSc Biomedische Technologie

Assessing Motoneuron Model Optimization and Parameter Sensitivity by Gamma-Factor

R.A.E. Mooiweer

Examination Committee
R.E. Ornelas Kobayashi, MSc.
Prof. dr. ir. M. Sartori
dr. S.U. Yavuz

January, 2024

DEPARTMENT OF BIOMECHANICAL ENGINEERING
University of Twente

ABSTRACT

The physiological properties of alpha-motoneurons (MNs) can be estimated by computational models. These models represent a person-specific tool for the assessment of neuronal adaptations after spinal cord injury (SCI). This study characterizes the sensitivity of MN model parameters and evaluates changes in the model optimization set-up to maximize the performance of neural data-driven optimization frameworks for capturing the *in vivo* firing characters of human MNs in healthy conditions. The model performance is assessed by a spike-by-spike comparison metric called gamma-factor. While an extended region of optimization and additional filtering techniques did not yield significant improvements to the simulated spike train derived from experimental data, the study reveals that the sensitivity of gamma-factor to model parameters is dependent on the size of the MN. These findings contribute to the development of computational tools translatable to the clinical setting for assessing lesion-specific adaptations and neurorehabilitation interventions.

KEYWORDS

Neuronal modeling, alpha-motoneuron, gamma-factor, optimization, sensitivity analysis

1 INTRODUCTION

Spasticity is a prevalent condition experienced by 65% of patients following spinal cord injury (SCI) [1]. It is characterized by a velocity-dependent increase in muscle tone [2] and hyperreflexia, as indicated by studies based on H- and stretch-reflexes assessment [3][4].

Following neuronal lesion, alpha-motoneurons (MNs) undergo physiological adaptations, including imbalance in ionic mechanisms [5], changes in size [6] and phenotype remodelling [7]. Although these adaptations have been indicated as the underlying mechanisms for the symptoms, non-invasive assessment is challenging. In this context, computational models represent a person-specific tool for the assessment of neuronal adaptations after neuronal lesion and effective neurorehabilitation interventions.

The central nervous system regulates movement by modulation of alpha-MNs. Alpha-MNs are key elements for the control of skeletal muscle contraction [8]. They are distributed in muscle-specific pools along the ventral horn of the spinal cord. The axons of alpha-MNs protrude outside of the vertebrae and into the periphery, innervating effector skeletal muscles by synapsing on extrafusal muscle fibers.

A single alpha-MN can innervate multiple muscle fibers, thereby creating the motor unit [9]. In the coordination of voluntary movement, a pool of MNs receives a shared common synaptic input (CSI) [10]. This CSI effectively filters out independent inputs, and its low-frequency components are linearly transformed into the neural drive controlling muscle activation [11].

The response of each MN to the CSI depends on its membrane properties. The action potential of the MN is produced through either synaptic or junctional neurotransmission [12], resulting in modified membrane permeability to certain ions. This triggers a cascade that enables the inflow of sodium ions, depolarizing the

membrane until its firing threshold and a subsequent repolarization to the resting potential by the outflow of potassium ions [8]. Once initiated, the action potential propagates along the length of the axon until reaching the neuromuscular junction (ie., synapse with the muscle membrane), resulting in muscle contraction [13].

Modeling the ionic conductance mechanisms provides a non-invasive way for estimating MN properties. Hodgkin and Huxley [14] established equations to characterize the firing dynamics of a MN based on its conductance properties. They described the activation and inactivation of sodium, potassium and leakage channels in an electrical circuit. Extensions of this model differ in level of detail by inclusion of multiple compartments and more ion channels (e.g., persistent calcium and sodium channels in the dendrites) [15], and generalizations of action potential generation [16][17] to decrease computational load.

Several studies involving animal preparations [18][19] have shown that parameter optimization of such models enable reproducing firing characteristics recorded *in vitro*. Furthermore, advanced signal processing techniques allow the non-invasive reconstruction of *in vivo* spike trains from human subjects via decomposition of high-density electromyography (HD-EMG) recordings. A widely used decomposition algorithm [20][21][22][21] is convolution kernel compensation blind-source separation [23]. This method defines a filter per MN to capture its contribution to the EMG signal. The convolution between each filter and its corresponding source (i.e., MN spike train) is calculated after which the filter weights are iteratively adjusted to improve the match between the convolution and the recorded EMG signal.

MN spike trains derived this way often undergo a quality-control stage to filter out non-physiologically realistic MNs. This is assessed based on their pulse-to-noise ratio (PNR), average discharge rate (DR) and coefficient of variation (CoV) [20].

Previous studies performed a person-specific estimation of soma diameter and slow potassium channel dynamics of *in vivo* spike trains decoded from the tibialis anterior muscle of healthy human subjects [24]. They optimized the model parameters by matching spike events between experimental and model spike trains, by means of a metric called gamma-factor [16]. This metric measures the probability that the model spike trains occur at the same time as experimentally observed. However, this spike-per-spike comparison involved solely the central spikes of a spike train. With this approach, the recruitment and derecruitment spiking characteristics are ignored during optimization, while derecruitment features are especially important in spasticity, because of self-sustained firing [25].

Furthermore, their parameter selection during optimization should be evaluated to gain insight into the model sensitivity to additional ion channels. This knowledge enables the application of this framework to SCI subjects, in which the ionic conductance mechanisms are disturbed.

Moreover, the optimization results are highly related to the quality of the decomposition. The spike trains fulfilling the quality control criteria may still include identification errors arising from

decomposition limitations [26]. These disturbances in the spike trains may lead to poor optimizations of MN parameters when fitting experimental data, because of the spike-per-spike comparison.

This project aimed at characterizing the sensitivity of model parameters to the gamma-factor. Additionally, this work evaluated how the performances of the MN model optimization framework is influenced by additional processing of the experimental data on spike train level and enlarging the optimization window.

Altogether, this work provides further insight into the sensitivity of MN model parameters and changes in the optimization set-up to maximize the performance of neural data-driven optimization frameworks for capturing the *in vivo* firing characters of human MNs in healthy and impaired conditions. Thus contributing to the development of computational tools translatable to the clinical setting for assessing lesion-specific adaptations and neurorehabilitation interventions.

2 METHODS

2.1 Experimental Setup

Four subjects (age 27.4 ± 2.07 years, weight: 70 ± 12.34 kg, height: 173.6 ± 10.06 cm) with no known neurological disorders were included in this study [24].

The task involved an isometric ankle dorsiflexion to study the tibialis anterior (TA). Subjects were seated in a Biodex chair (M4 Biodex Medical Systems Inc., Shirley, NY, USA) and asked to perform ramp-and-hold contractions at target forces of 10, 20, 30, 40 and 50% of their maximum voluntary contraction (MVC). The rate of force was set to 20% MVC/s for both reaching the ramp plateau and returning back to the resting state. The targets for the force-tracking task were presented to the subjects in real-time, together with feedback about the task performance. Each condition was performed five times.

Torque and HD-EMGs from the TA were simultaneously recorded using an in-house developed acquisition interface. The HD-EMG was measured using an 8×8 electrode grid and a TMSi Refa multi-channel amplifier (TMS International B. V., Oldenzaal, The Netherlands) at a sampling frequency of 2048 Hz. Torque was recorded using a National Instruments Data Acquisition card (NI DAQ) at a sampling frequency of 512 Hz.

2.2 Decomposition

The HD-EMGs were band-pass filtered between 20 and 500 Hz using a zero-phase Butterworth filter. The filtered signals were decomposed into individual MN spike trains by convolution kernel compensation blind-source separation [23]. The spike trains underwent a quality-control algorithm [20] in which MNs with a PNR > 20 dB, CoV > 0.3 and average DR > 30 Hz were excluded from the further study.

2.3 Computational model

This study builds upon the model described in [24], where person-specific conductance-based models of a single compartment were established to represent MNs. They included the conductance of leakage (g_l), sodium (g_{Na}), slow potassium (g_{Ks}) and fast potassium (g_{Kf}) channels to simulate the neuronal ionic mechanisms. Voltage-dependent

ion channels were described using a pulse-based model approach [17], where the opening and closing of each specific ion channel is described by the rate constants alpha (α_i) and beta (β_i). The subscript i denotes the gating variables m , h , n , and q for respectively sodium activation (α_M , β_M), sodium inactivation (α_H , β_H), fast potassium activation (α_N , β_N) and slow potassium activation (α_Q , β_Q) [17].

Additionally, the model included soma diameter (D_s), membrane resistance (R_m) and membrane capacitance (C_m).

To account for the person-specificity, an excitability factor ΔI was calculated for each subject [24]. This factor functions as a gain factor to translate the neural drive into the CSI.

The parameters were obtained by a double single-objective optimization, as explained in [24]. Firstly, the error in first-spike time was minimized by optimizing D_s . Secondly, β_Q and α_Q were obtained by minimizing differences in gamma-factor (Section 2.4). All parameters not explicitly mentioned here were set to their default values [27] throughout the optimization.

2.4 Coincident Spike-Match

Coincidence-factor Γ (1) is a measure to quantify the coincidence of spikes between experimental and simulated spike trains [16]. A value of one corresponds to identical spike trains, whereas zero denotes complete randomness. The spiking coincidences in MNs with $\Gamma < 0.1$ where considered random chance [22].

To obtain the parameters resulting in the highest Γ , the value of (1) was maximized by minimizing (2) throughout the optimization.

$$\Gamma = \frac{2}{1 - 2\delta f_e} \left(\frac{n_c - 2\delta f_e n_e}{n_e + n_m} \right) \quad (1)$$

$$2 \left| \frac{f_e - f_m}{f_e} \right| - \Gamma \quad (2)$$

In (1) and (2) n_e and n_m denote the number of spike events in respectively the experimental and simulated spike trains. The number of coincident spikes is represented by n_c . The coincidence check was performed within a time window (δ) of 2 ms around each experimental spike, because this is the approximate duration of an action potential in cortical neurons [28]. f_e and f_m represent the mean firing frequencies during the plateau phase of the exercise.

2.5 Spike Correction

After the quality-control algorithm filtered the MNs based on PNR, CoV and average DR, the further analysis focused on evaluating the individual spikes within the spike trains based on the interspike intervals (ISIs). This assessment aimed to measure the dispersion of spikes from the central distribution of discharge rates.

Unrealistic ISIs in the experimental data may arise from merged spike trains of different MNs after decomposition (i.e., identification errors [26]). Therefore, a pre-optimization spike processing algorithm (referred to as Spike Correction) was established (Fig. 1) to account for spike omissions and spurious firings [29] based on the probability density function (PDF) of the ISIs of decomposed spike trains. A gamma distribution [30] was fit to the experimental ISIs by using MATLAB's (The MathWorks, Inc., Natick, MA, USA) function *fitdist*. This function uses an optimization algorithm to

maximize the likelihood of the observed data being generated from a gamma distribution.

The acceptable ISIs boundaries were defined by selecting the first and last 10% of the cumulative distribution function (CDF) per spike train. This percentage was chosen based on a manual evaluation of the filter performance. Subsequently, the spike trains were evaluated to identify ISIs outside this range. Accordingly, large ISIs resulting from spurious firings and small ISIs resulting from spike omissions, were both neglected from calculating the mean discharge rate. For checking coincident spikes, spurious firings were accounted for by neglecting the second spike of large ISIs.

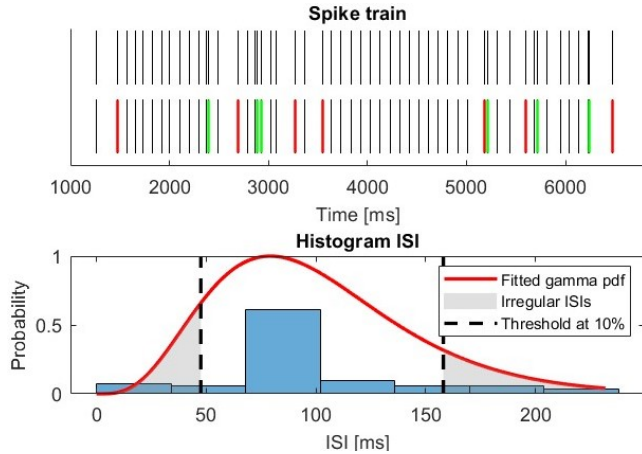


Figure 1: Procedure to identify irregular ISIs. A gamma PDF is fitted to the experimental ISIs. The first and last 10% of the CDF is filtered out. In green the second spikes of small ISIs, resulting from spurious firings, are indicated. In red the second spike of large ISIs, resulting from spike omissions.

2.6 Sensitivity Analysis

To investigate the influence of the model parameters on gamma-factor, a sensitivity analysis (SA) was performed using MATLAB's SAFE Toolbox for Global Sensitivity Analysis [31].

Parameter selection. Since D_s defines MN recruitment through the optimization of first-spike time error [22], and is therefore excluded from the second optimization stage (Section 2.4), the SA considered only the β_i and α_i of the ionic channels. Due to motor-unit type specific parameter ranges and firing dynamics [32] [27] [24], the SA was performed on a representative sample from each of the three MN types: a low-, medium- and high-threshold MN (i.e., S-, FR, FF-type), in which, generally, the first has the smallest D_s and the latter has the largest one.

Accordingly, the SA included 6 parameters ($M=6$): $\beta_Q, \alpha_Q, \beta_N, \alpha_N, \beta_H, \alpha_H$ were sampled based on PDFs adjusted for each MN type following the parameter ranges described in [32]. The PDFs were constructed as a normalized distribution around the midpoint of the range (Table 1) with 95% of the values falling within one standard deviation (Appendix, Fig. A6).

To account for interdependencies between MN parameters, the AAT (All-At-a-Time) [33] sampling strategy was used. This method

involved randomly varying the parameter values simultaneously, while keeping track of the values of the parameter of interest. The resulting sensitivity index includes the direct influence of that parameter as well as the influence due to interdependencies.

PAWN. As gamma-factor does not yield a unimodal and non-skewed distribution [33], the SA was performed using the distribution-based PAWN method [34]. Unlike traditional variance-based methods [35], this method involved deriving the sensitivity indices moment independently by using the entire gamma-factor distribution. Accordingly, the gamma-factor distribution was characterized by approximating the CDF instead of the PDF to avoid tuning parameters (e.g., the bin width) and to reduce computational costs, because the CDF follows directly from the obtained gamma-factor.

Gamma-factor was obtained by evaluating the model for each parameter combination and comparing the simulated spike train with a reference spike train. This reference spike train was manually generated by running the model with a predefined set of parameters (Table 1). This way, the spike trains generated by the model are able to produce the same pattern as the reference spike train (i.e., gamma-factor = 1), which may not be the case for a for *in vivo* decomposed spike train.

Fig. 2 illustrates the steps to find the sensitivity indices. The sensitivity to each parameter (x_i) is estimated by calculating the difference between an unconditional CDF and n conditional CDFs [34]. The unconditional CDF is constructed by finding N_u parameter combinations, varying all parameters simultaneously. To investigate the influence of the M parameters, each parameter is assigned n conditioning values within its range. For each conditioning value, the model is evaluated for N_c parameter combination in which all parameters except x_i are varied. Per conditioning point a conditional CDF is constructed from the N_c gamma-factors.

The sample sizes (N_u, n and N_c) were based on a trade-off between computational load and sufficient convergence of the results. They were chosen on a trial-and-error basis, by trying different sample size combinations as recommended in [36].

Interpretation. The difference between unconditional and conditional curves was quantified by computing the Kolmogorov-Smirnov statistic (KS), which is the normalized maximum vertical distance (MVD) between the two CDFs [34]. Throughout this paper, the

Table 1: Parameter values for constructing the reference spike trains and centering the sample space PDFs. Adapted from [32] by taking the midpoint of their specified ranges. The D_s values are the midpoint of the size clusters in [24].

Parameter	Unit	Parameter values		
		S-type	FR-type	FF-type
D_s	μm	47	106.5	177
β_Q	ms^{-1}	0.0315	5.5315	16.5125
α_Q	ms^{-1}	1.5000	6.6250	16.8750
β_N	ms^{-1}	0.1000	5.5750	16.5250
α_N	ms^{-1}	1.5000	1.6250	16.8750
β_H	ms^{-1}	4.0000	8.5000	17.5000
α_H	ms^{-1}	0.5000	5.8750	16.6250

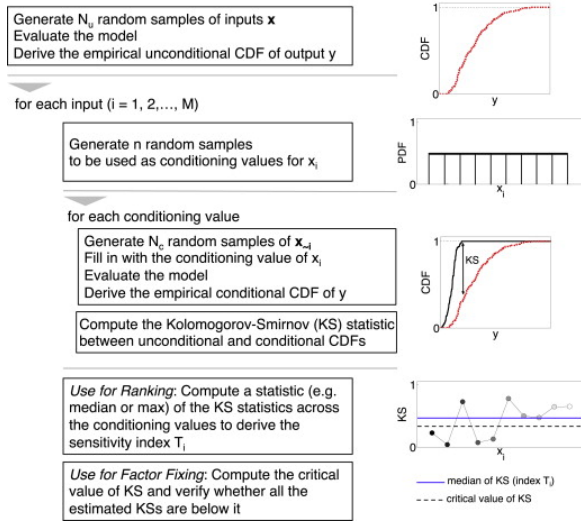


Figure 2: Workflow of PAWN method. y is the model output (i.e., gamma-factor). x_i are the parameters that are sampled within their specific distributions (Appendix, Fig. A6). The unconditional CDF (red) is constructed from N_u random parameter combinations and compared with the n conditional CDFs (black, here only one shown) constructed from N_c systematic parameter combinations. Copied from [34].

term MVD was used instead of KS to avoid confusion with the slow potassium channels K_s .

The sensitivity index of a parameter was computed from the maximum MVD [34]. The confidence bounds of the sensitivity indices were derived by subsampling the conditional and unconditional gamma-factors per CDF to construct a new CDF [37]. Each CDF was reconstructed 500 times based on these subsets. Consecutively, the new MVD values were calculated and a new MVD statistic was subsequently extracted. This MVD statistic is the sensitivity index from which the variability is examined across the different subsamples. The variability provides insights into the uncertainty associated with the SA results. Parameters with a confidence level < 0.05 were considered non-influential [34].

2.7 Analysis

Different tests were performed to analyse the results of the changes to the optimization framework and the SA.

Test 1: Optimization window for coincidence. Test 1 evaluated the difference of optimizing gamma-factor taking the entire ramp length vs only the plateau section. This analysis was performed taking a representative sample of four MNs per target MVC, including the first- and last-recruited MNs and two in between (Appendix, Fig. A1). After the two optimizations, gamma-factor was computed both at plateau phase (Γ_{plateau}) and total length (Γ_{total}). Furthermore, for both optimization conditions derecruitment time error, derecruitment DR error and recruitment DR error were quantified. Additionally, the resulting parameter values (i.e., optimized for each of the two conditions) were evaluated by studying the differences.

Test 2: Spike correction. The second test evaluated the influence that the spike processing algorithm (Section 2.5), applied to the *in vivo* spike trains, had on the optimization performance. Both irregular large and small ISIs were neglected in calculating the mean frequencies in (2). Additionally, the second peak of the small ISIs was removed during the optimization of Γ , as well as in calculating N_e . The optimization was performed once with and once without implementing the spike-correction, for the same MNs as in Test 1. The optimizations were compared by calculating Γ_{plateau} and evaluating the difference in parameter values.

For Test 1 and Test 2 the model was optimized for the same three parameters as in [24]: the soma diameter D_s and opening and closing rate constants α_Q and β_Q for activation of slow potassium ion channels. These parameters were optimized following the optimization framework established in [22]. This was performed on experimental data of one subject only because of computational load.

Test 3: Sensitivity Analysis. To investigate how much the parameter selection during optimization influenced gamma-factor, a PAWN SA was performed in Test 3. This involved evaluating the sensitivity of β_Q , α_Q , β_N , α_N , β_H and α_H for S-, FR and FF-type MNs separately. Different sample sizes were used to investigate convergence. To evaluate the repeatability of the SA, one SA was performed twice with the same sample sizes.

Test 4: SA-based parameter optimizations. Based on the SA of Test 3, Test 4 involved performing optimizations with different sets of parameters for the same MNs as in Test 1 and Test 2. The parameter sets included different combinations of the parameters which showed significant sensitivity indices. The optimization performance was evaluate by comparing the obtained spike trains by gamma-factor and the trend of their instantaneous DRs (iDR). This evaluation was conducted separately for the different MN size types.

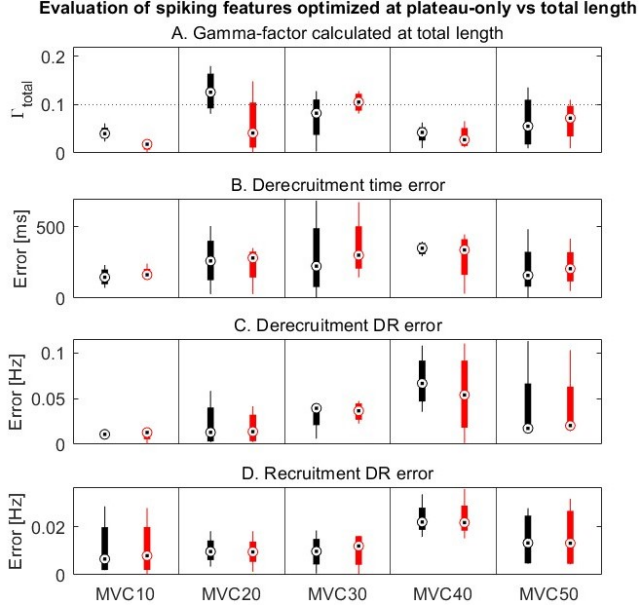


Figure 3: Evaluation of gamma-factor, derecruitment time error, derecruitment DR error and recruitment DR error when changing the window of parameter optimization from plateau phase (black) to total ramp length (red). Per MVC condition the mean of four MNs is calculated. A: The dotted line represents the randomness threshold below which the spike-match is considered random. The presented gamma-factors were calculated over the total ramp length. C, D: DRs were calculated during the initial and last second of spiking.

3 RESULTS

3.1 Optimization Window for Coincidence

In line with *Test 1*, Fig. 3A displays that Γ_{total} improved for spike trains of 30% and 50% MVC. The individual MNs (Appendix, Fig. A2) showed an increase in 5, decrease in 10 and no change in 5 out of 20 MNs. In both optimizations, the vast majority of MNs was not above the threshold of randomness.

The mean error values did not vary much between the two optimizations (Fig. 3B, C and D). The error in derecruitment time between the modelled and the experimental spike trains more frequently increased (12 out of 20) than decreased (7 out of 20) after optimizing at total length (Appendix, Fig. A3). For derecruitment DR error, this ratio was 9 versus 10. There was no consistent relationship between an increased Γ_{total} and a decrease in the other spiking feature errors.

For the recruitment DR error, the distribution of the mean values was approximately the same for both optimizations within a MVC condition (Fig. 3D), which resulted from a small change per MN (Appendix, Fig A3).

For β_Q and D_s minor changes in parameter values were observed between the two optimizations (Fig. 5). The values for α_Q showed more significant variations with respect to the range of observed parameter values.

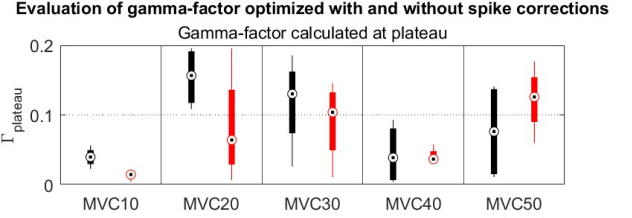


Figure 4: Evaluation of gamma-factor with (red) and without (black) correction of spikes during parameter optimization. Per MVC condition the mean of four MNs was calculated. The dotted line represents the randomness threshold below which the spike-match was considered random. The presented gamma-factors were calculated at the plateau phase.

3.2 Spike Correction

Fig. 4 displays the resulting $\Gamma_{plateau}$ of *Test 2*. Only in 50% MVC, a significant increase in the mean value was observed. $\Gamma_{plateau}$ increased in 7 and decreased in 12 out of 20 MNs. There was no consistent relationship between the CoV (Appendix, Fig. A1) and the change of $\Gamma_{plateau}$ (Appendix, Fig. A4).

Fig. 5b shows similar patterns as Fig. 5a. The change in D_s was very limited and α_Q varied the most between the two optimizations. Although the mean variation in β_Q was approximately the same as in Fig. 5a, some exceptions were observed with larger differences.

3.3 Sensitivity Analysis

The results of *Test 3* are shown in Fig. 6 and 7.

A high sensitivity was observed for the lower values of β_i . Furthermore, the shape of the CDFs showed that for S-type, the tuning of β_i allows for a more frequent reaching of higher gamma-factors.

In all MN types, the conditioning point corresponding to the reference spike train (vertical dotted lines, Fig. 7) resulted in a low sensitivity, except for β_Q and β_N in S-type.

The sensitivity indices (Fig. 6) show a similar pattern for S- and FR-type, displaying that gamma-factor was most sensitive to β_i . For FF-type, the sensitivity of β_N was lower than in S- and FR-type, while α_Q was higher.

Appendix Fig. A8, A9 and A10 include a comparison of different sample sizes. The regional sensitivity within the parameter space was observed at lower sample sizes as well. Both the smoothness of the CDFs and the convergence of the sensitivity indices increased with sample size. Although the exact values of these indices showed some variations, a recurring pattern was seen in the relative contribution of the parameters within one MN type.

Appendix Fig. A11 highlights the repeatability of a SA. Even though different conditioning points were used, still the same shapes of regional sensitivity within the parameter space were present.

Some gamma-factors were observed multiple times in the SA (Appendix, Fig. A7). The corresponding parameter values had a wide spread distribution, whereas the corresponding DR errors occurred in the same range.

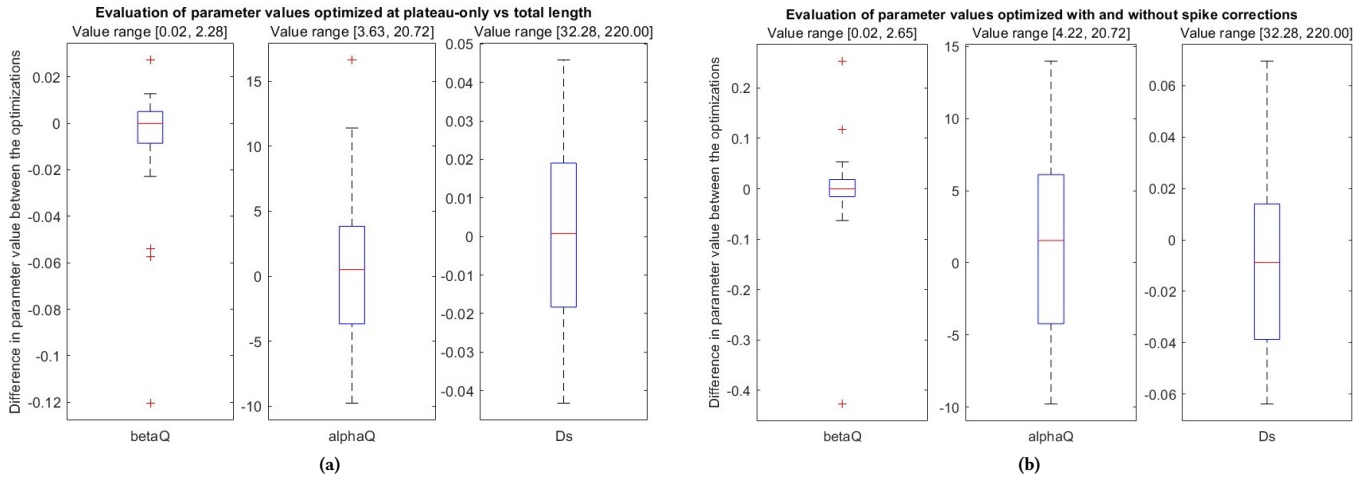


Figure 5: Evaluation of parameter values when changing the window of parameter optimization from plateau phase to total ramp length (a) or performing the optimization with and without correction (b). The difference in parameter values between the two optimizations was computed per MN. The absolute parameter value ranges are indicated to put the differences into perspective.

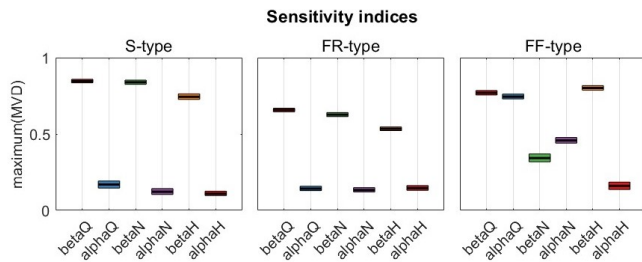


Figure 6: Sensitivity of gamma-factor to different parameters. Sensitivity indices were obtained by taking the maximum of the MVDs in Fig. 7.

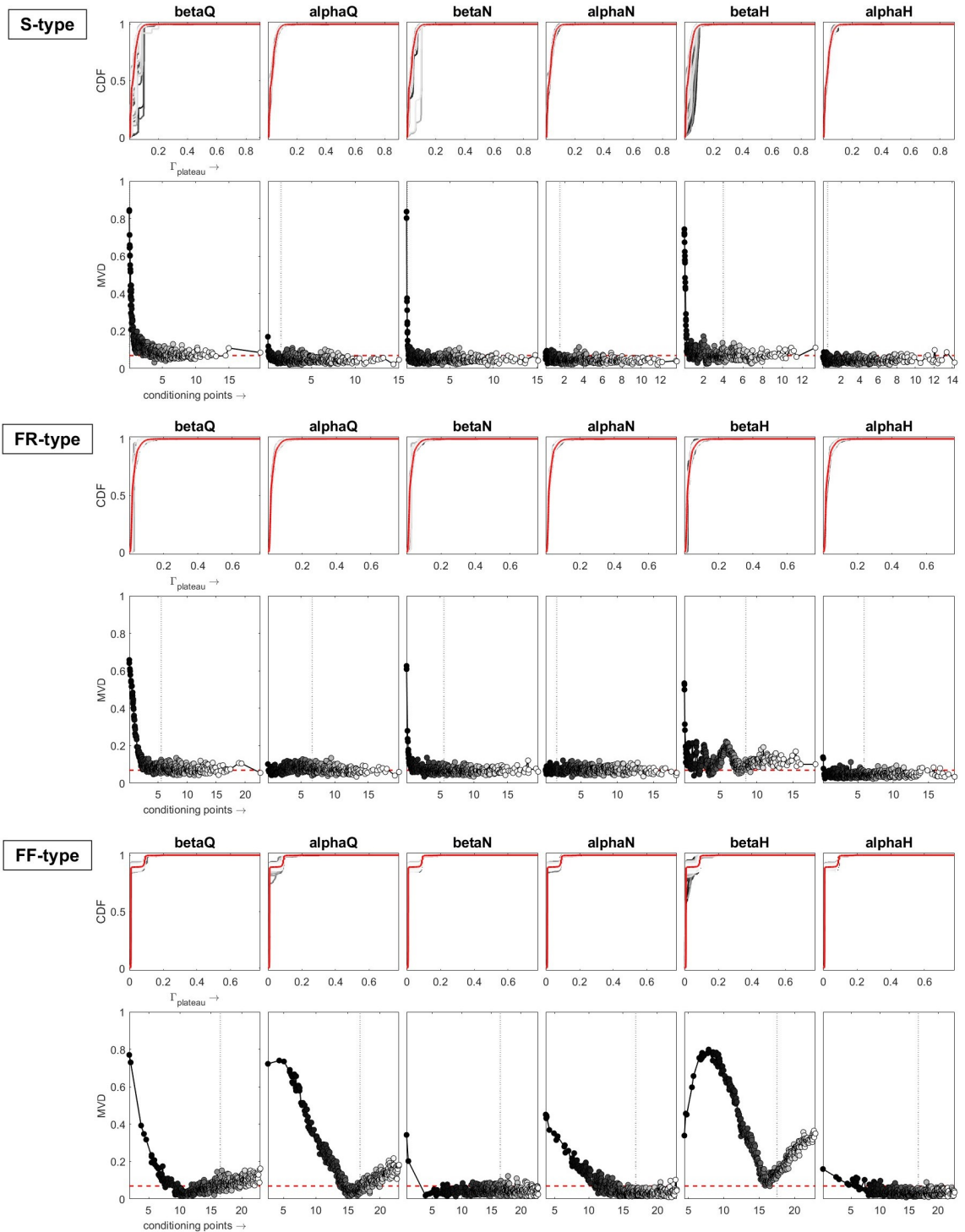


Figure 7: MVD values corresponding to each conditional curve for the different MN types. The unconditional CDF is indicated in red. The color of the conditional CDFs (grey) is similar to the corresponding conditioning point. The red (dashed) threshold indicates the 0.05 confidence level. The vertical dotted lines show the parameter values used for the reference spike train. Results obtained with $N_u = 10\,000$, $n = 400$, $N_c = 400$. A comparison of different sample sizes is included in Appendix Fig. A8, A9 and A10.

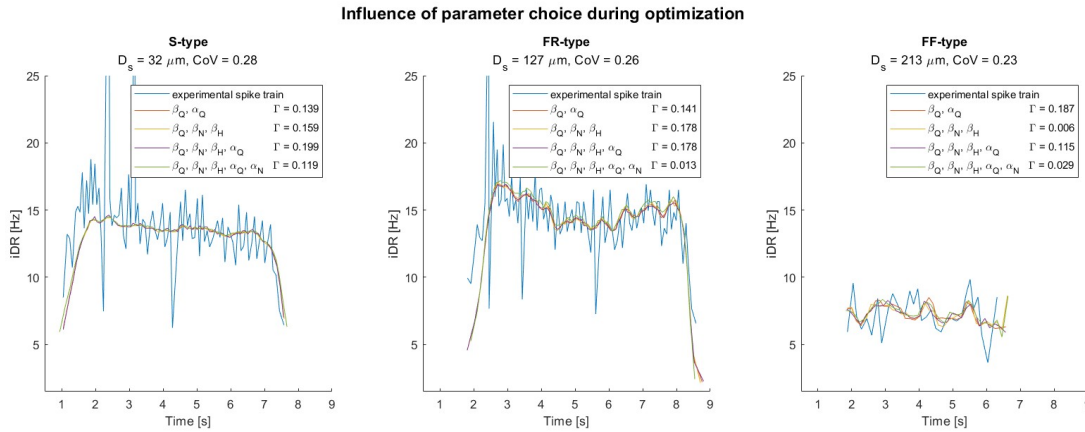


Figure 8: Comparison of the spike trains obtained from different parameter optimizations by instantaneous DR (iDR). For each size cluster the outcomes of one MN are presented, with the corresponding gamma-factors per optimization. D_s is the mean value of all optimizations and the denoted CoV corresponds to the experimental spike train.

3.4 SA-based Parameter Optimizations

Fig. 8 and 9 show the comparison of the different parameter optimizations of *Test 4*.

The different parameter choices had a small effect on the course of the iDRs (Fig. 8). Although gamma-factor varied, the overall spiking pattern did not change much compared to the experimental graph. The recruitment and derecruitment features, in terms of lower iDRs, were less observed in the FF-type MNs.

Gamma-factor demonstrated significant variation across different optimizations (Fig. 9). For both S-type and FF-type, the mean gamma-factors indicated that the combination of β_Q , β_N , β_H and α_Q outperformed the inclusion of α_N . Individual MN analysis revealed that for FF-type, in general, the highest gamma-factors were achieved by the combination of β_Q , β_N , β_H and α_Q (Appendix, Table A1).

Influence of parameter choice on gamma-factor

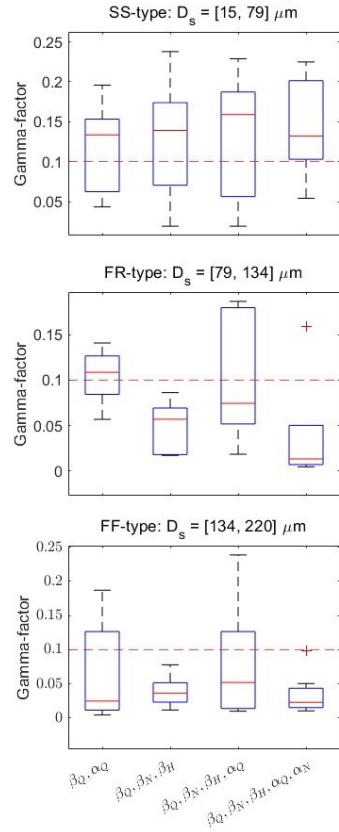


Figure 9: Comparison of the model performance by gamma-factor based on different parameters during optimization. The MNs used in Section 3.1 and 3.2 are clustered based on their soma diameter.

4 DISCUSSION

In this study different aspects of gamma-factor as a measure of model performance were investigated. This involved exploring changes in the set-up of the optimization framework and performing a sensitivity analysis on selected model parameters.

4.1 Optimization Window for Coincidence

It was expected that optimization based on all present spikes would result in a better model performance. However, in the majority of MNs this was not the case. In most cases where Γ_{plateau} decreased, Γ_{total} decreased as well, probably because they both cover the plateau phase of the ramp. Contrary to what might be expected, Γ_{plateau} (Appendix, Fig. A2) sometimes increased as well after enlarging the optimization window to total ramp length.

The recruitment DR error is affected the least by the change of optimization window. This may be due to the recruitment threshold being set in the first step of the optimization procedure by D_s . This is the reason for the minor change in D_s between the different optimizations as well. Changes in D_s are not related to the different optimization approaches, but could only be the result of the intrinsic variability of metaheuristic optimization.

The fluctuations in α_Q and β_Q were studied before in [24]. They found that optimizing a MN under the same conditions can yield quite different values for α_Q and minor changes in β_Q . Our findings, resulting from optimization of a MN under different conditions, align with these observations (Fig. 5a). From this analysis the influence of β_Q on gamma-factor can thus be concluded. To evaluate the current parameter selection used to optimize the coincident spike-match, a SA was performed.

From these results, it can be concluded that optimizing over the plateau or the entire ramp length, does not consistently improve model performance or significantly change the model parameters. A larger optimization window, however, does come with a increase in computational time. Therefore, it is suggested to optimize over the plateau phase only.

4.2 Spike Correction

Regarding the parameter changes between the optimizations with and without spike correction, the same patterns can be observed for D_s and α_Q (Fig. 5a) as for the change of optimization window (Fig. 5b).

The detection of irregular ISIs was unbiased except for the 10% boundaries. The ignorance of these irregular ISIs in calculating the mean discharge frequency seemed reasonable. The question remains, however, if it can be justified to delete the spurious firings when checking the coincident spike-match. The choice to delete the second spike from a small ISI and not the first, was unsubstantiated. It would have been better to statistically investigate which spike fitted better in the total spike train pattern.

Another critical point in the identification of these spike omissions and spurious firings is that the difference between ramp trajectories were not taken into account. The DR during recruitment and derecruitment is lower than during the constant force delivery at the plateau [38]. With the current approach, the 10% boundaries were determined over the total ramp length. Consequently, in some spike trains the recruitment and derecruitment spikes were filtered

out (Appendix, Fig. A5). A better approach would have been to base the PDF fitting only on plateau phase and not filter the ascending and descending ramp phases.

Furthermore, fitting a gamma distribution is only possible in the case of a low CoV_{ISI} [39]. In spasticity, there is a higher variability in spiking frequencies [40], for example because of sustained firing [25]. As a result, an additional peak will be encountered in the ISI distribution, resulting from the self-sustained firing. This means that additional steps should be taken to fit a distribution function.

Throughout the study, the MVC conditions were split to investigate differences in the gamma-factor. These difference were expected based on the different time span of recruitment and derecruitment, because of the 20% MVC/s ramp speed during the ascending and descending part of the ramp (0.5, 1.0, 1.5, 2.0, 2.5 s respectively). Because the plateau phase has the same duration of 5s in all conditions, the proportion of the derecruitment and recruitment features in higher MVC conditions is higher.

Unfortunately, this difference in recruitment and derecruitment duration was forgotten to take into account in calculating the DR during recruitment and derecruitment (Fig. 3C and D). For all conditions this was done during the initial and last second of spiking, whereas this should have been adjusted to the rate of recruitment and derecruitment. For example, the last second of spiking in the MVC10 condition also includes a portion of the plateau phase and is thus biased.

Implementation of the spike correction more often decreased than increased gamma-factor, thus suggesting that this change is not beneficial for the optimization performance.

The choice for only one subject and the limited number of studied MNs (4 MNs per condition) was made because of computational limitations, but does not allow for drawing reliable conclusions or observing trends. With the same amount of MNs, it would have been better to focus on one MVC condition, and in a later stage investigate the differences between the different MVC conditions. Furthermore, because the PAWN results show that the sensitivity is dependent on the MN size, studying the gamma-factor results per MN size-cluster could also give us valuable information. This should be handled with care, because boundaries between the size-clusters are not clear-cut.

Moreover, the repeatability of every optimization should be investigated to conclude the effect of the implemented change more reliably. This becomes particularly important when increasing the number of parameters to be optimized, because the number of possible combinations will grow. This will give insight in the uniqueness of the solutions.

4.3 Sensitivity Analysis

Given the sample size comparison and repeatability of the SA results, the chosen sample sizes ($N_u = 10\,000$, $n = 400$, $N_c = 400$) were sufficient to reach convergence of the sensitivity indices. However, the frequently observed gamma-factors (Appendix, Fig. A7) could influence the CDF curves. The high occurrence of a specific gamma-factor causes sharp transitions in the CDF curve. Since this repetition of gamma-factor showed little relationship with the corresponding parameter combinations, the shift of the curve did

not imply something about the parameters sensitivity but overestimated the MVD.

From Fig. 7 it can be concluded that the average influence of α_Q on gamma-factor is minimal. Non-influential parameters have their MVD values all below the confidence level, indicating that the conditional CDFs are approximately the same as the unconditional CDF and thus have the same gamma-factor distribution. It is important to keep in mind that a high MVD does not directly imply a higher gamma-factor, as the MVD is an absolute measure and does not imply anything about the relative positioning between the unconditional and conditional curves.

The overall observed higher sensitivity of β_i than α_i aligns with the parameter differences observed in Fig. 5, where α_Q showed more variation than β_Q . In the context of action potential dynamics, α and β describe the opening and closing rate of voltage-dependent ion channels respectively [41]. This implies that the model is sensitive to the closing of Na⁺ channels, which terminates the depolarization, and the closing of K⁺ channels, which terminates the refractory period. The model is less sensitive to the opening rate of these channels.

The pulse-based model used in this study, describes the ion channels dynamics of an action potential by pulses triggered when the membrane potential exceeds the firing threshold [17]. Within the pulse-based model, the ion channel dynamics are modelled by an exponential relationship between β_i and α_i . The values of β_i and α_i describe the height of, either negative or positive, rectangular pulses. The parameters α_Q , α_N and β_H are related, because their values influence the channel dynamics during the action potential. On the other hand, β_Q , β_N and α_H influence the behaviour in between to action potentials.

With this knowledge, it is thus expected that the sensitivity of the parameters within one group are related, but this was not observed in Fig. 6.

The regional sensitivity to the lower parameter values suggest that slow closing rates, which cause a longer depolarization and refractory period, have a significant influence on the model performance.

The larger FF-type MNs had an additional high sensitivity to α_Q , indicating the importance of the opening rate of slow potassium channels. This may be to account for the lower DRs, as observed in Fig. 8. The slow potassium channels play a role in the afterhyperpolarization phase [42], in which the firing rates are determined by controlling the refractory period.

An interesting observation is that the model optimizations returns low β_Q values (Fig. 5) that are not within the ranges of [32] (Table 1). This skewness of the β_Q distribution to the lower values, was also observed in [24] in which a larger number of MNs was investigated. These low β_Q values suggest a low closing rate of the slow potassium channels, resulting in a longer action potential duration [43].

The question arises whether the PDF spaces used in the SA should be implemented in the optimization framework as well, to obtain more representative (e.g., higher β_Q) values.

The sampling space for the parameter values was constrained by a PDF to increase the probability of finding combinations of parameter values that were within the MN type [32]. Because of the PDF, the conditioning points of, for example, FF-type were all

above 4 ms^{-1} (Fig. 7). Since the maximum of most MVD values was observed at the lower values, it would be interesting to see if even higher sensitivities are achieved when sampling the lower conditioning points as well.

4.4 SA-based Parameter Optimizations

FF-type MNs exhibited a high α_Q sensitivity (Fig. 6). Inclusion of α_Q indeed appeared to result in higher gamma-factors (Fig. 9 and Appendix Table A1). To validate the alignment between the outcomes of the model optimizations and the SA results, future research should perform a confirmation by exclusion of parameters. This is particularly important for β_Q , since this parameter was currently included in all optimizations.

For S- and FR-type MNs, the comparison of gamma-factor between the different optimizations did not reveal a trend (Appendix, Table A1).

The absence of recruitment and derecruitment features (e.g., lower DRs) in the larger MNs (Fig. 8) is probably because of a miscalculation of the CoV while applying the quality control criteria. The CoV was based on all present spikes, whereas this should have been based on the central spikes only [44]. Therefore, the CoV indicated in A1 were overestimated. This also means that the selection of MNs is biased towards the spike trains in which the difference between the DR at plateau and the DR during recruitment and derecruitment is small.

Gamma-factors for FF-type MNs were on average lower than for the smaller sized MNs (Fig. 9). Combined with the results of the SA, in which different sensitivity indices were found for FF-type than for S- or FR-type, this suggest a distinct optimization approach for the different MN types. Based on the D_s value obtained in the first step of the optimization protocol, a different parameter combination or different parameter ranges should be used in the second optimization step. Again, these ranges should be handled with care, because boundaries between the size-clusters are not clear-cut.

Furthermore, the parameters that are not optimized were currently set to a default value independent of the MN size, it should be considered to adjust these default values per size cluster as well.

Optimization based on more parameters requires re-calibration of the optimization framework, which was not undertaken in this study. Nevertheless, it can be observed that the mean discharge rate and the overall pattern of recruitment and derecruitment features were incorporated in the model in all optimizations (Fig. 8).

From Fig. 8 it can be concluded that, although the gamma-factors varied, the different parameter combinations during optimization did not influence the overall spiking pattern much. This is an important observation regarding the suitability of using gamma-factor to evaluate the model performance. The possible cause for these large fluctuations in gamma-factor and frequently observed low values is illustrated in Fig. 8. The experimental spike trains had some exceptional variations in the discharge rate.

The optimization with and without spike corrections (Section 3.2) addressed this problem. The iDR course of these optimizations showed a small difference when correcting for these unpredictable iDRs as well (Appendix, Fig. A12). Since the most influential parameter value β_Q did not vary much (Fig. 5b), the optimization

framework seems to nullify these unpredictable iDRs already by optimizing Formula 2 in which the mean DR is incorporated. Therefore, it might be better to base future comparisons on Formula 2 instead of gamma-factor (Formula 1) and explore other metrics to assess model performance.

4.5 Spasticity

The main goal in this field of study is to establish tools for the assessment and treatment of neuronal lesions. This study looked into different aspects of optimizing gamma-factor as a metric to fit a neurocomputational model to experimental data.

To evaluate the suitability of the PAWN methodology in neurocomputational modeling applications, this work prioritized working with healthy subjects and a single-compartment model of the soma to investigate the changes of gamma-factor. Since the clinical application of this study field is to establish models representing spasticity, further research should evaluate this sensitivity in two-compartment models [32][27] as well. These models have two coupled compartments, representing the soma and a dendrite.

The importance of including a dendritic compartment lies in the inclusion of calcium-dependent potassium, persistent calcium and persistent sodium currents [45], which play a role in spasticity [46]. They are involved in the generation of plateau potentials, which is a membrane potential from which, after initiation, a neuron can fire without the need of a depolarizing current [25]. If the plateau threshold is reached, certain voltage-gated channels get activated, resulting in a persistent inward current (PIC). This manifests in self-sustained firing, which causes hyperreflexia as one of the main mechanisms responsible for spastic symptoms.

Therefore, future research should perform the SA for two-compartment models and should investigate the contribution of other ion channels and currents as well.

5 CONCLUSION

This work contributes to the state of the art in the field of neurocomputational models by new insights in the optimal setup to perform parameter optimizations.

Additional processing techniques as filtering the spike train and enlarging the region of optimization lead to fluctuating gamma-factors. Nevertheless, the effect on both the parameter values and the overall spiking features were insignificant and non-consistent. These additional steps add to a higher computational load, thus it is advised to exclude these steps to reduce the execution time of the model.

A sensitivity analysis into the selection of parameters to be optimized showed different results depending on the MN size. However, these results were not prominently visible in the optimizations with different parameter combinations.

From the observation that various gamma-factors lead to approximately the same spike train we can question the suitability of gamma-factor as a metric to evaluate model performance. It is therefore advised to explore alternative evaluation criteria to assess the model performance.

The validity of these conclusions can be argued, remarking that they are based on a small number of observations.

This work provides a methodology for studying the model sensitivity to different model parameters. Working towards models to represent MNs of spastic subjects, further research should include additional parameters (e.g., calcium channel dynamics) and implementation of two-compartment models.

REFERENCES

- [1] K. A. Holtz, R. Lipson, V. K. Noonan, B. K. Kwon, and P. B. Mills, "Prevalence and Effect of Problematic Spasticity After Traumatic Spinal Cord Injury," *Arch. Phys. Med. Rehabil.*, vol. 98, no. 6, pp. 1132–1138, Jun. 2017, issn: 0003-9993. doi: 10.1016/j.apmr.2016.09.124.
- [2] J. W. Lance, "The control of muscle tone, reflexes, and movement: Robert Wartenberg Lecture," *Neurology*, vol. 30, no. 12, pp. 1303–1313, Dec. 1980, issn: 0028-3878. doi: 10.1212/wnl.30.12.1303. eprint: 7192811.
- [3] M. R. W. Angel, "The H Reflex in Normal, Spastic, and Rigid Subjects: Studies," *Arch. Neurol.*, vol. 8, no. 6, pp. 591–596, Jun. 1963, issn: 0003-9942. doi: 10.1001/archneur.1963.00460060021002.
- [4] J. B. Nielsen, N. T. Petersen, C. Crone, and T. Sinkjaer, "Stretch Reflex Regulation in Healthy Subjects and Patients with Spasticity," *Neuromodulation: Technology at the Neural Interface*, vol. 8, no. 1, pp. 49–57, Jan. 2005, issn: 1094-7159. doi: 10.1111/j.1094-7159.2005.05220.x.
- [5] C. J. Heckman, M. Johnson, C. Mottram, and J. Schuster, "Persistent inward currents in spinal motoneurons and their influence on human motoneuron firing patterns," *Neuroscientist*, vol. 14, no. 3, pp. 264–275, Jun. 2008, issn: 1073-8584. doi: 10.1177/1073858408314986. eprint: 18381974.
- [6] P. Bose, R. Parmer, P. J. Reier, and F. J. Thompson, "Morphological changes of the soleus motoneuron pool in chronic midthoracic contused rats," *Exp. Neurol.*, vol. 191, no. 1, pp. 13–23, Jan. 2005, issn: 0014-4886. doi: 10.1016/j.expneurol.2004.08.028. eprint: 15589508.
- [7] G. Sheean, "The pathophysiology of spasticity," *Eur. J. Neurol.*, vol. 9, no. Suppl, pp. 13–19, May 2002, issn: 1351-5101. doi: 10.1046/j.1468-1331.2002.0090s1003.x. eprint: 11918643.
- [8] D. Purves, G. J. Augustine, W. C. Hall, A.-S. LaMantia, and L. E. White, "Neuroscience," in 5th ed. Sinauer, 2012, ch. 16, isbn: 9780878935895.
- [9] C. J. Heckman and R. Enoka, *Physiology of the motor neuron and the motor unit*. Dec. 2004, vol. 4, isbn: 978-0-44451359-5. doi: 10.1016/S1567-4231(04)04006-7.
- [10] C. J. De Luca and Z. Erim, "Common drive of motor units in regulation of muscle force," *Trends Neurosci.*, vol. 17, no. 7, pp. 299–305, Jul. 1994, issn: 0166-2236. doi: 10.1016/0166-2236(94)90064-7.
- [11] D. Farina, F. Negro, and J. L. Dideriksen, "The effective neural drive to muscles is the common synaptic input to motor neurons," *J. Physiol.*, vol. 592, no. 16, pp. 3427–3441, Aug. 2014. doi: 10.1113/jphysiol.2014.273581.
- [12] R. K. Goyal and A. Chaudhury, "Structure activity relationship of synaptic and junctional neurotransmission," *Autonomic neuroscience : basic & clinical*, vol. 176, no. 0, p. 11, Jun. 2013. doi: 10.1016/j.autneu.2013.02.012.
- [13] D. V. Roberts, "THE ANATOMY AND PHYSIOLOGY OF THE NEUROMUSCULAR JUNCTION," *Br. J. Anaesth.*, vol. 35:510-20. Sep. 1963, issn: 0007-0912. doi: 10.1093/bja/35.9.510. eprint: 14066100.
- [14] A. L. Hodgkin and A. F. Huxley, "A quantitative description of membrane current and its application to conduction and excitation in nerve," *J. Physiol.*, vol. 117, no. 4, p. 500, Aug. 1952. doi: 10.1113/jphysiol.1952.sp004764.
- [15] P. F. Pinsky and J. Rinzel, "Intrinsic and network rhythmogenesis in a reduced Traub model for CA3 neurons," *J. Comput. Neurosci.*, vol. 1, no. 1-2, pp. 39–60, Jun. 1994, issn: 0929-5313. doi: 10.1007/BF00962717. eprint: 8792224.
- [16] C. Clopath, R. Jolivet, A. Rauch, H.-R. Lüscher, and W. Gerstner, "Predicting neuronal activity with simple models of the threshold type: Adaptive Exponential Integrate-and-Fire model with two compartments," *Neurocomputing*, vol. 70, no. 10, pp. 1668–1673, Jun. 2007, issn: 0925-2312. doi: 10.1016/j.neucom.2006.10.047.
- [17] A. Destexhe, "Conductance-based integrate-and-fire models," *Neural Comput.*, vol. 9, no. 3, pp. 503–514, Apr. 1997, issn: 0899-7667. doi: 10.1162/neco.1997.9.3.503. eprint: 9097470.
- [18] A. Rauch, G. La Camera, H.-R. Luscher, W. Senn, and S. Fusi, "Neocortical pyramidal cells respond as integrate-and-fire neurons to in vivo-like input currents," *J. Neurophysiol.*, vol. 90, no. 3, pp. 1598–1612, Sep. 2003, issn: 0022-3077. doi: 10.1152/jn.00293.2003. eprint: 12750422.
- [19] *Simulation of dendritic Cav1.3 channels in cat lumbar motoneurons: Spatial distribution*, [Online; accessed 21. Dec. 2023], Dec. 2005. doi: 10.1152/jn.00391.2005.
- [20] A. Gogea-cochea, A. Kuck, E. van Asseldonk, et al., "Interfacing With Alpha Motor Neurons in Spinal Cord Injury Patients Receiving Trans-spinal Electrical Stimulation," *Front. Neurol.*, vol. 11, p. 528 464, Jun. 2020, issn: 1664-2295. doi: 10.3389/fneur.2020.00493.
- [21] L. B. R. Orssatto, D. N. Borg, A. J. Blazevich, R. L. Sakugawa, A. J. Shield, and G. S. Trajano, "Intrinsic motoneuron excitability is reduced in soleus and tibialis

- anterior of older adults,” *GeroScience*, vol. 43, no. 6, p. 2719, Dec. 2021. doi: 10.1007/s11357-021-00478-z.
- [22] “Optimization framework for the model-based estimation of in vivo motoneuron properties in the intact human,” in *2021 43rd Annual International Conference of the IEEE Engineering in Medicine Biology Society (EMBC)*, United States: IEEE, Dec. 2021, pp. 6126–6129, ISBN: 978-1-7281-1180-3. doi: 10.1109/EMBC46164.2021.9630260.
- [23] A. Holobar, M. A. Minetto, and D. Farina, “Accurate identification of motor unit discharge patterns from high-density surface EMG and validation with a novel signal-based performance metric,” *Journal of Neural Engineering*, vol. 11, no. 1, p. 016008, Feb. 2014, ISSN: 1741-2552. doi: 10.1088/1741-2560/11/1/016008. eprint: 24654270.
- [24] R. Ornelas-Kobayashi, A. Gogeascoechea, and M. Sartori, “Person-specific biophysical modeling of alpha-motoneuron pools driven by in vivo decoded neural synaptic input,” English, *IEEE transactions on neural systems and rehabilitation engineering*, vol. 31, pp. 1532–1541, Mar. 2023, ISSN: 1534-4320. doi: 10.1109/TNSRE.2023.3247873.
- [25] O. Kiehn and T. Eken, “Functional role of plateau potentials in vertebrate motor neurons,” *Curr. Opin. Neurobiol.*, vol. 8, no. 6, pp. 746–752, Dec. 1998, ISSN: 0959-4388. doi: 10.1016/S0959-4388(98)80117-7.
- [26] J. C. Kline and C. J. De Luca, “Error reduction in EMG signal decomposition,” *J. Neurophysiol.*, vol. 112, no. 11, p. 2718, Dec. 2014. doi: 10.1152/jn.00724.2013.
- [27] R. R. L. Cisi and A. F. Kohn, “Simulation system of spinal cord motor nuclei and associated nerves and muscles, in a Web-based architecture,” *J. Comput. Neurosci.*, vol. 25, no. 3, pp. 520–542, Dec. 2008, ISSN: 1573-6873. doi: 10.1007/s10827-008-0092-8. eprint: 18506610.
- [28] R. Jolivet, R. Kobayashi, A. Rauch, R. Naud, S. Shinomoto, and W. Gerstner, “A benchmark test for a quantitative assessment of simple neuron models,” *J. Neurosci. Methods*, vol. 169, no. 2, pp. 417–424, Apr. 2008, ISSN: 0165-0270. doi: 10.1016/j.jneumeth.2007.11.006.
- [29] X. Hu, W. Z. Rymer, and N. L. Suresh, “Assessment of validity of a high-yield surface electromyogram decomposition,” *J. NeuroEng. Rehabil.*, vol. 10, p. 99, 2013. doi: 10.1186/1743-0003-10-99.
- [30] F. Gabbiani and S. J. Cox, “CHAPTER 11 - Probability and Random Variables,” in *Mathematics for Neuroscientists*, Cambridge, MA, USA: Academic Press, Jan. 2010, pp. 155–173, ISBN: 978-0-12-374882-9. doi: 10.1016/B978-0-12-374882-9.00011-3.
- [31] F. Pianosi, F. Sarrazin, and T. Wagener, “A Matlab toolbox for Global Sensitivity Analysis,” *Environ. Model. Software*, vol. 70, pp. 80–85, Aug. 2015, ISSN: 1364-8152. doi: 10.1016/j.envsoft.2015.04.009.
- [32] L. A. Elias and A. F. Kohn, “Individual and collective properties of computationally efficient motoneuron models of types S and F with active dendrites,” *Neurocomputing*, vol. 99, pp. 521–533, Jan. 2013, ISSN: 0925-2312. doi: 10.1016/j.neucom.2012.06.038.
- [33] F. Pianosi, K. Beven, J. Freer, et al., “Sensitivity analysis of environmental models: A systematic review with practical workflow,” *Environ. Model. Software*, vol. 79, pp. 214–232, May 2016, ISSN: 1364-8152. doi: 10.1016/j.envsoft.2016.02.008.
- [34] F. Pianosi and T. Wagener, “A simple and efficient method for global sensitivity analysis based on cumulative distribution functions,” *Environ. Model. Software*, vol. 67, pp. 1–11, May 2015, ISSN: 1364-8152. doi: 10.1016/j.envsoft.2015.01.004.
- [35] T. Homma and A. Saltelli, “Importance measures in global sensitivity analysis of nonlinear models,” *Reliab. Eng. Syst. Saf.*, vol. 52, no. 1, pp. 1–17, Apr. 1996, ISSN: 0951-8320. doi: 10.1016/0951-8320(96)00002-6.
- [36] F. Pianosi and T. Wagener, “Distribution-based sensitivity analysis from a generic input-output sample,” *Environ. Model. Software*, vol. 108, pp. 197–207, Oct. 2018, ISSN: 1364-8152. doi: 10.1016/j.envsoft.2018.07.019.
- [37] T. Efron, *An Introduction to the Bootstrap*. Andover, England, UK: Taylor & Francis, May 1994, ISBN: 978-0-42924659-3. doi: 10.1201/9780429246593.
- [38] C. J. De Luca and Z. Erim, “Common drive of motor units in regulation of muscle force,” *Trends Neurosci.*, vol. 17, no. 7, pp. 299–305, Jul. 1994, ISSN: 0166-2236. doi: 10.1016/0166-2236(94)90064-7. eprint: 7524216.
- [39] F. Gabbiani and S. J. Cox, “CHAPTER 15 - Quantification of Spike Train Variability,” in *Mathematics for Neuroscientists*, Cambridge, MA, USA: Academic Press, Jan. 2010, pp. 237–249, ISBN: 978-0-12-374882-9. doi: 10.1016/B978-0-12-374882-9.00015-0.
- [40] M. A. Gorassini, M. E. Knash, P. J. Harvey, D. J. Bennett, and J. F. Yang, “Role of motoneurons in the generation of muscle spasms after spinal cord injury,” *Brain*, vol. 127, no. Pt, p. 10, Oct. 2004, ISSN: 1460-2156. doi: 10.1093/brain/awh243. eprint: 15342360.
- [41] P. Dayan and L. F. Abbott, *Theoretical neuroscience : computational and mathematical modeling of neural systems*. Cambridge, MA, USA: Cambridge, Mass. : Massachusetts Institute of Technology Press, 2001., 2001, ch. 5, ISBN: 978-026204199.
- [42] M. Duméniéu, N. Fourcaud-Trocmé, S. Garcia, and N. Kuczewski, “Afterhyperpolarization (AHP) regulates the frequency and timing of action potentials in the mitral cells of the olfactory bulb: role of olfactory experience,” *Physiological Reports*, vol. 3, no. 5, May 2015. doi: 10.14814/phy2.12344.
- [43] B. Rudy, “Diversity and ubiquity of K channels,” *Neuroscience*, vol. 25, no. 3, pp. 729–749, Jun. 1988, ISSN: 0306-4522. doi: 10.1016/0306-4522(88)90033-4. eprint: 2457185.
- [44] S. Andreassen and A. Rosenfalck, “Regulation of the firing pattern of single motor units.” *J. Neurol. Neurosurg. Psychiatry*, vol. 43, no. 10, p. 897, Oct. 1980. doi: 10.1136/jnnp.43.10.897.
- [45] J. Graham, V. Booth, and R. Jung, “Modeling motoneurons after spinal cord injury: Persistent inward currents and plateau potentials,” *Neurocomputing*, vol. 65–66, pp. 719–726, 2023, ISSN: 0925-2312. doi: 10.1016/j.neucom.2004.10.067.
- [46] A. M. Gutman, “BISTABILITY OF DENDRITES,” *Int. J. Neural Syst.*, vol. 01, no. 04, pp. 291–304, Jan. 1991, ISSN: 0129-0657. doi: 10.1142/S0129065791000339.

APPENDIX

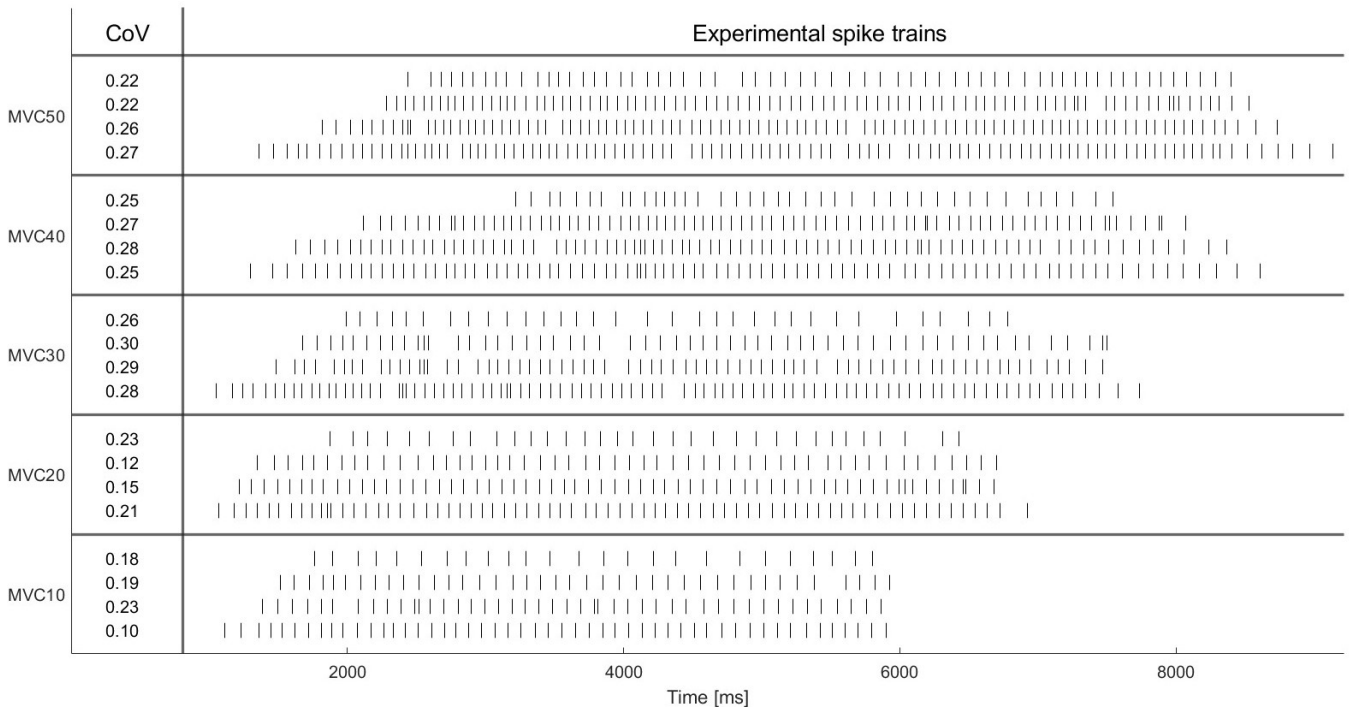


Figure A1: Overview of the experimental spike trains used throughout the optimizations. Per MVC condition 4 MNs were selected, including the first- and last-recruited MNs and two in between. The CoV_{ISI} of each spike train is printed on the left.

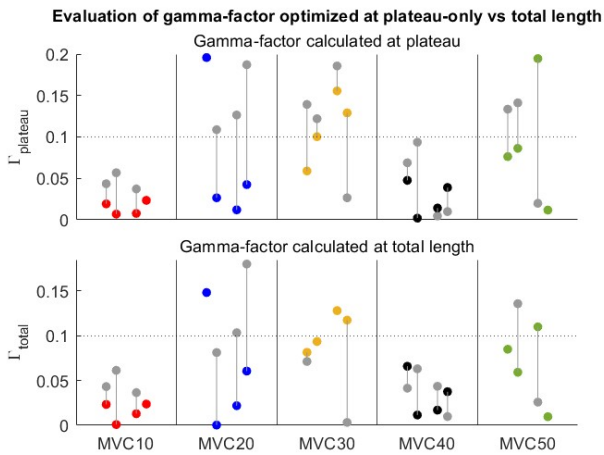


Figure A2: Evaluation of gamma-factor when changing the window of parameter optimization from plateau phase (gray) to total ramp length (colored) per MN. Per MVC condition four MNs were investigated, including the first (rightmost) and last recruited (leftmost) and two MNs in between. The dotted line represents the randomness threshold below which the spike-match is considered random.

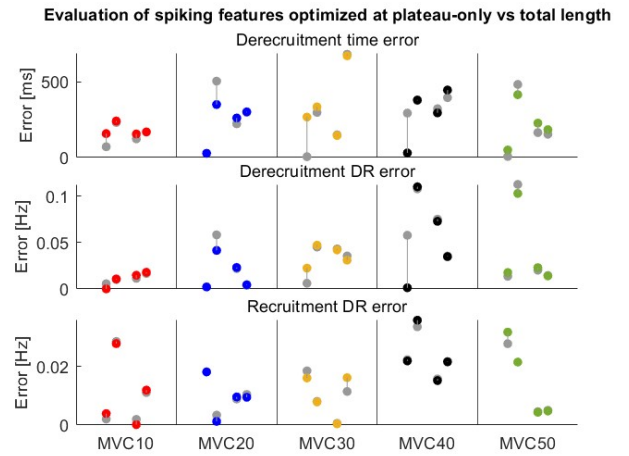


Figure A3: Evaluation of derecruitment time error, derecruitment DR error and recruitment DR error when changing the window of parameter optimization from plateau phase (gray) to total ramp length (colored) per MN. Per MVC condition four MNs were investigated, including the first (rightmost) and last recruited (leftmost) and two MNs in between. The DRs were calculated during the initial and last second of spiking.

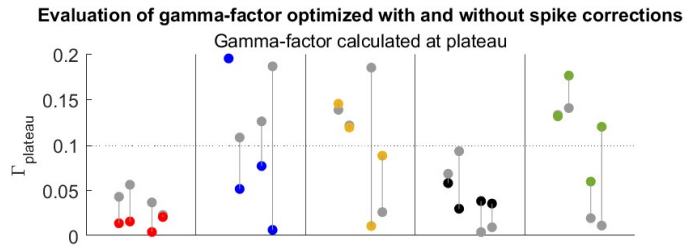


Figure A4: Evaluation of gamma-factor when changing the window of parameter optimization from plateau phase (gray) to total ramp length (colored) per MN. Per MVC condition four MNs were investigated, including the first (rightmost) and last recruited (leftmost) and two MNs in between. The dotted line represents the randomness threshold below which the spike-match is considered random.

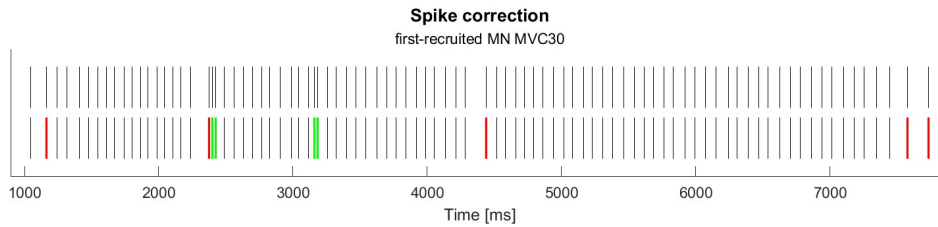


Figure A5: Spike train of the first-recruited MN of MVC30 after correcting for identification errors. The filtering algorithm seems to filter out the derecruitment spikes, because of the lower DR, which was not taken into account.

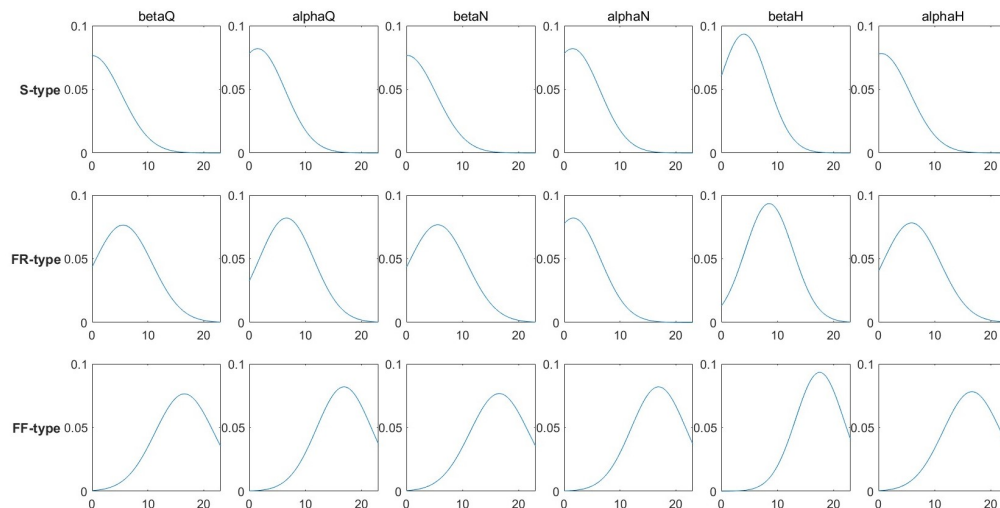


Figure A6: Sample spaces of parameter values for PAWN. Based on values in [32] as indicated by the peak values in Table 1

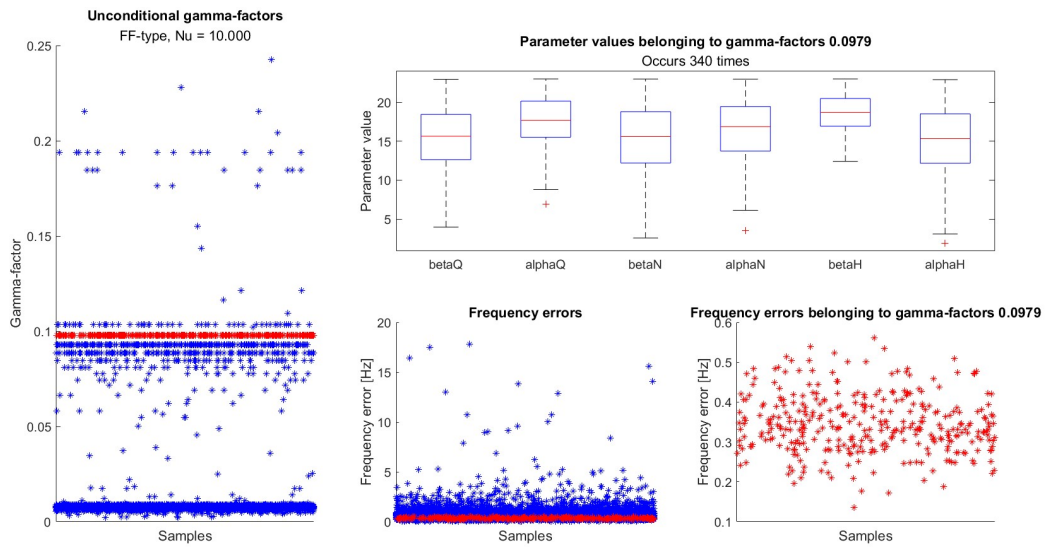


Figure A7: Example to illustrate the fact that several gamma-factors were observed multiple times. The corresponding parameter values showed a large spread, but the frequency (DR) errors were in the same range.

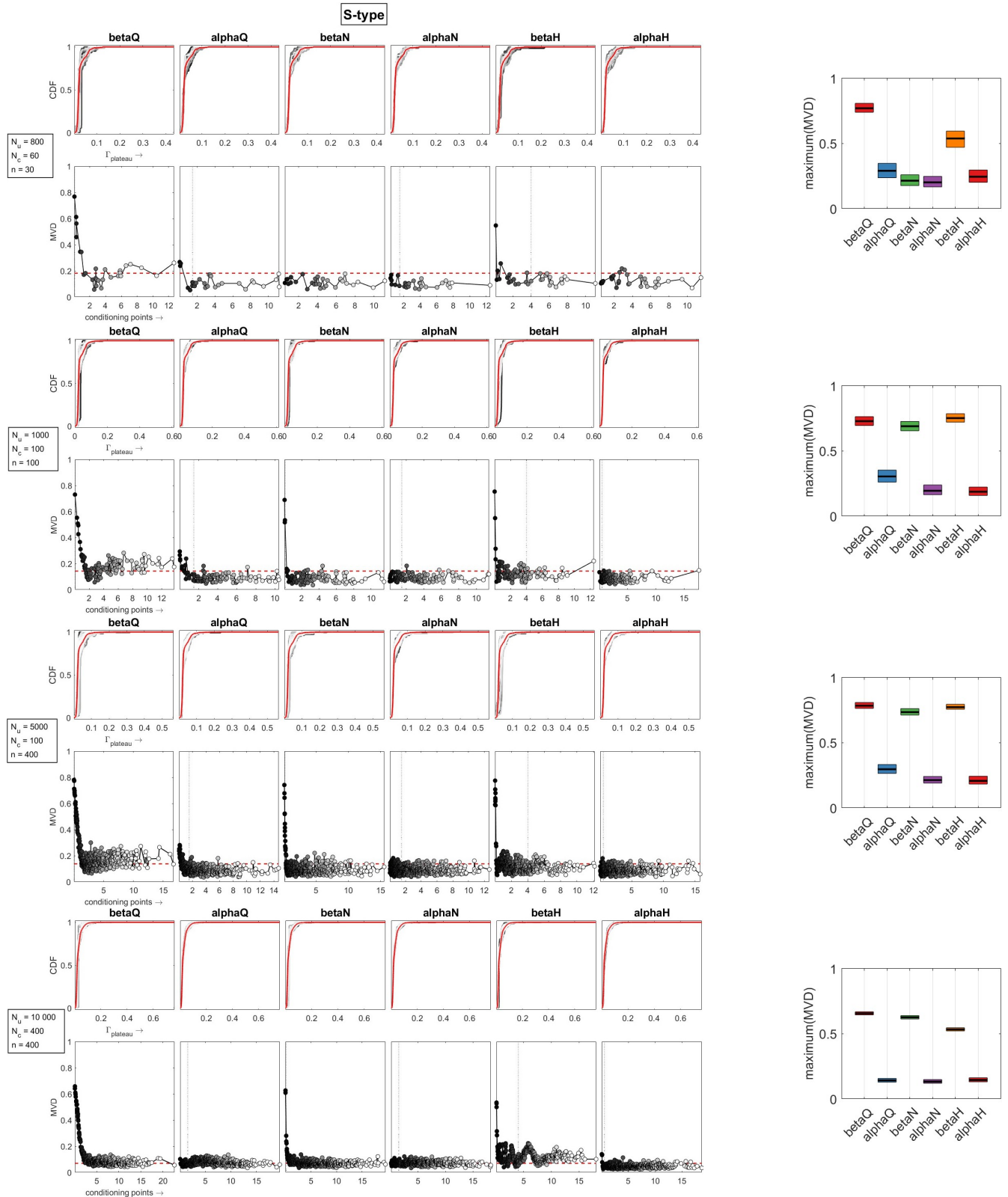
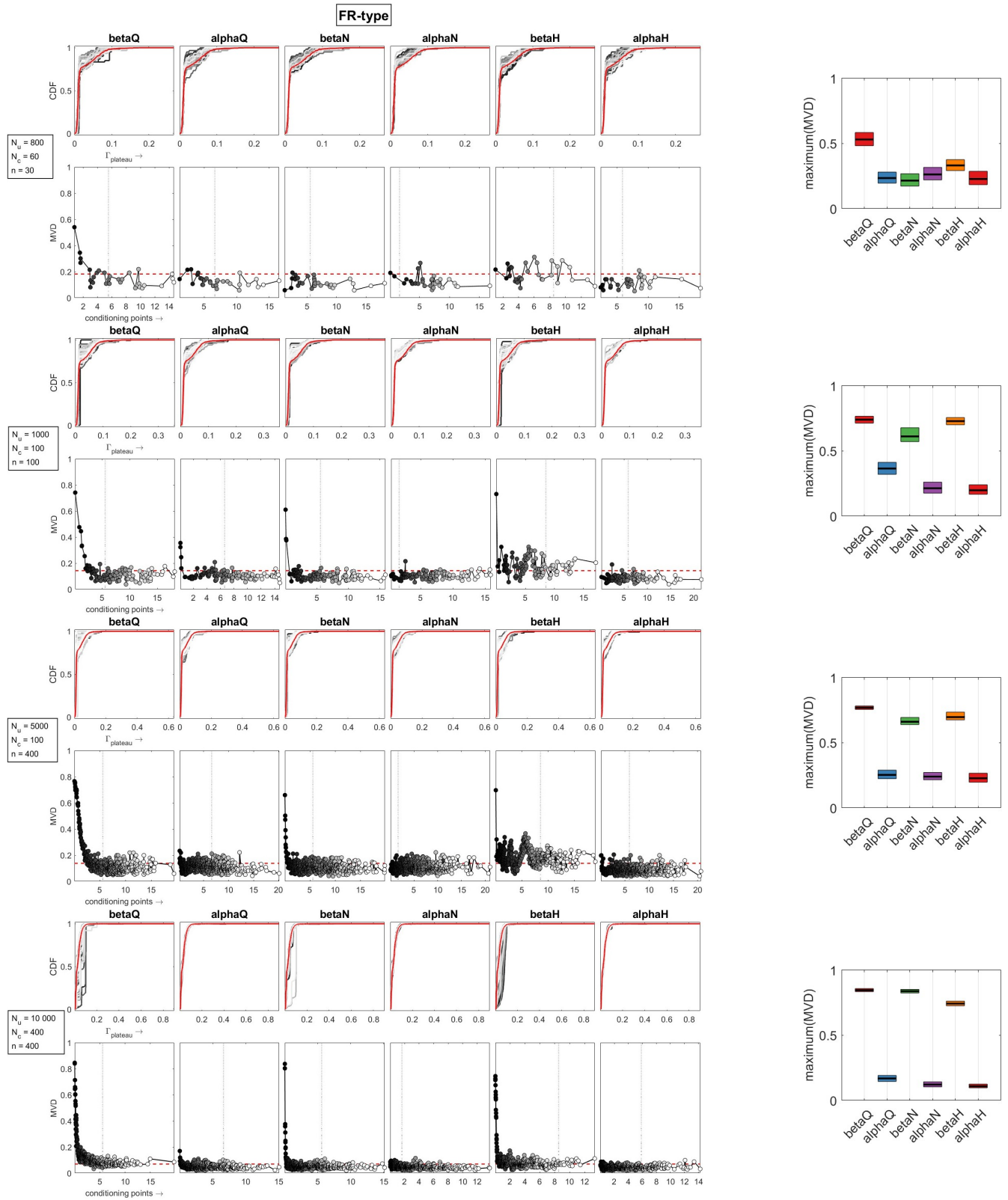
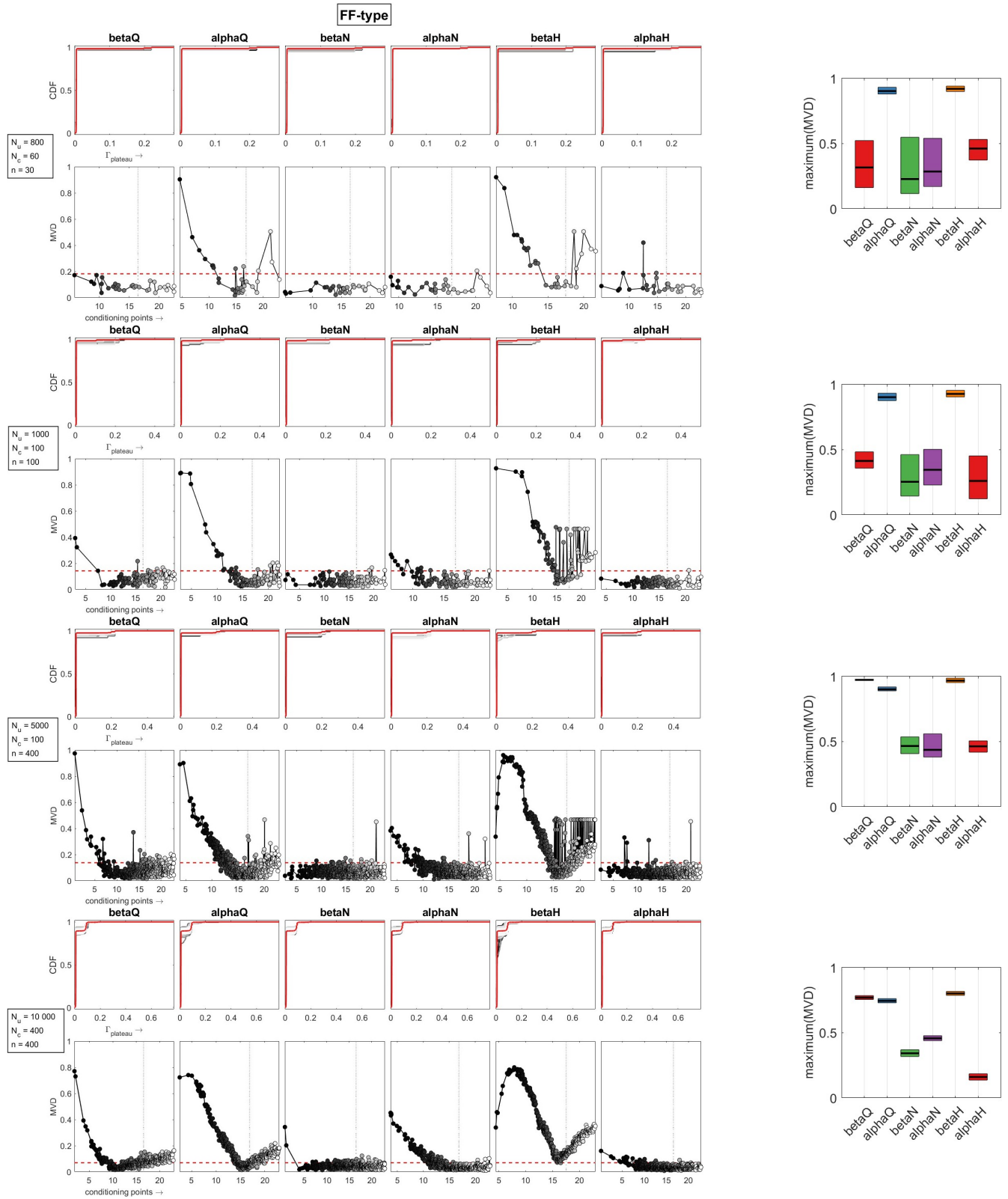


Figure A8: Comparison of different sample size combinations for S-type MN





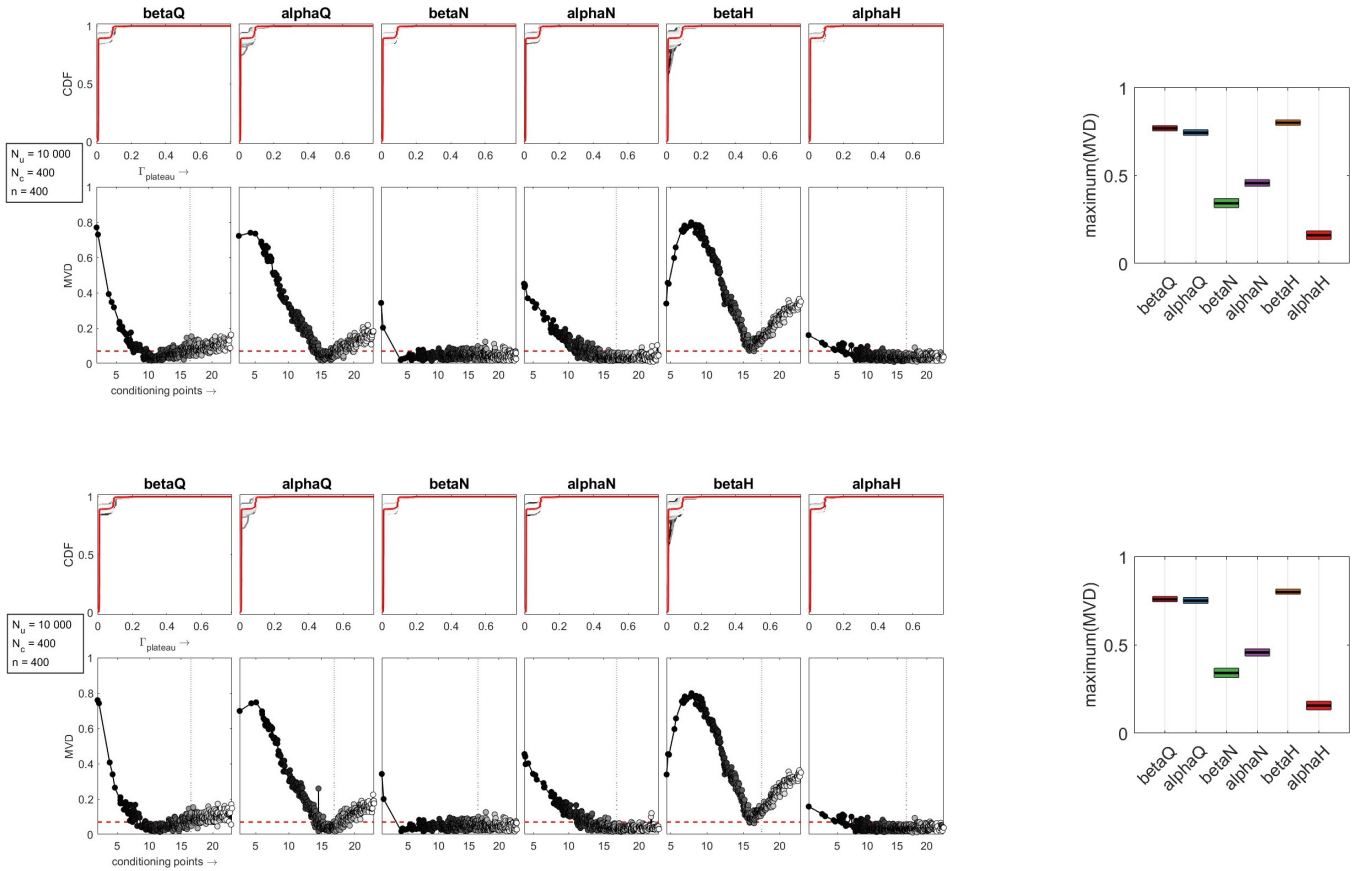


Figure A11: Repeatability of SA for FF-type MN

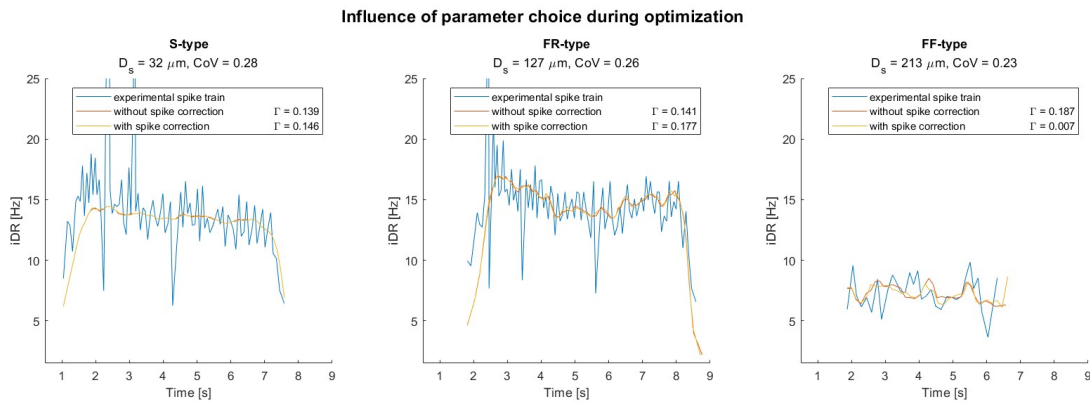


Figure A12: Comparison of the spike trains by instantaneous DR (iDR) after optimization with and without spike train corrections. For each size cluster the outcomes of one MN are presented, with the corresponding gamma-factors per optimization. D_s is the mean value of all optimizations and the denoted CoV corresponds to the experimental spike train.

Table A1: Gamma-factors resulting from the different parameter optimizations. MNs were sorted on D_s . The color shades were tuned for each MN to see which optimization resulted in the highest gamma-factors.

MN		Gamma-factor			
	D_s	β_Q, α_Q	$\beta_Q, \beta_N, \beta_H$	$\beta_Q, \beta_N, \beta_H, \alpha_Q$	$\beta_Q, \beta_N, \beta_H, \alpha_Q, \alpha_N$
S-type	32	0.139	0.139	0.159	0.119
	51	0.134	0.153	0.229	0.132
	61	0.044	0.019	0.019	0.054
	63	0.069	0.088	0.069	0.225
	65	0.196	0.238	0.173	0.194
FR-type	106	0.109	0.064	0.063	0.004
	121	0.122	0.057	0.187	0.014
	121	0.094	0.017	0.075	0.16
	123	0.057	0.018	0.018	0.008
	127	0.141	0.086	0.178	0.013
FF-type	137	0.127	0.043	0.127	0.015
	149	0.037	0.052	0.052	0.023
	165	0.186	0.045	0.239	0.011
	179	0.005	0.052	0.014	0.044
	187	0.02	0.078	0.157	0.098
	189	0.023	0.023	0.023	0.023
	209	0.012	0.012	0.012	0.012
	213	0.187	0.029	0.115	0.029
	214	0.027	0.027	0.052	0.051
	219	0.01	0.019	0.01	0.019